An Approximate integral method for calculating the diffracted component from multiple two-dimensional objects

Nightingale, T. R. T.

Journal of the Acoustical Society of America, 97, 1, pp. 51-61, 1995-01-01

An Approximate integral method for calculating the diffracted component from multiple two-dimensional objects

NRCC-35986

Nightingale, T.R.T.

January 1995

A version of this document is published in / Une version de ce document se trouve dans:
Journal of the Acoustical Society of America, 97, (1), pp. 51-61, January 01, 1995

An approximate integral method for calculating the diffracted component from multiple two-dimensional objects

T. R. T. Nightingale
Acoustics Laboratory, Institute for Research in Construction, National Research Council, Ottawa K1A 0R6, Canada

(Received 24 March 1993; accepted for publication 25 August 1994)

A method for determining the diffracted or scattered components due to the interaction of a wave with multiple two-dimensional objects is given. The method presented uses approximate boundary conditions to simplify the numerically cumbersome set of integral equations associated with nonapproximate analytic solutions of the Helmholtz integral. The approximate boundary conditions, defined here, are shown to decouple the N by N set of simultaneous equations. The approximate boundary conditions are used to calculate the insertion loss for various sizes of two-dimensional objects. The predictions are compared to measured results and limitations are discussed.

PACS numbers: 43.20.Fn

INTRODUCTION

The scattered field due to the presence of an object may be calculated by two groups of methods: approximate or analytic. Each group is formed from the Helmholtz integral equation. The limitations of each method is manifest in its formulation. These will be briefly discussed to illustrate the need for an alternate method that is capable of describing the diffracted field due to multiple two-dimensional objects, when the geometrical methods fail and when the computing time of the analytic methods becomes excessive.

The following is a list of acronyms that will be used throughout the discussions:

(1) KBC—Kirchhoff boundary conditions,
(2) HI—Helmholtz integral,
(3) HKI—Helmholtz–Kirchhoff integral,
(4) RKI—Rayleigh–Kirchhoff integral, and
(5) MKBC—modified Kirchhoff boundary conditions.

In this paper screens are two-dimensional objects or "thin" three-dimensional objects that can be considered as behaving like two-dimensional objects for the wavelengths considered.

There are two types of approximate methods: the geometrical theories of diffraction, and approximate integral solutions using the Kirchhoff boundary conditions. Each requires that a specific set of conditions be satisfied. The geometrical theories of diffraction (Keller's geometrical theory of diffraction,[1] and Kouyoujian and Pathak's uniform theory of diffraction[2]) which invoke a high-frequency approximation are restricted to objects that can be constructed from one or more semi-infinite half-planes. Description of scattered fields due to simple objects of finite extent using geometrical methods can lead to very substantial errors as the solution fails to converge if restrictions on object dimension, source–object, and object–receiver distances are not satisfied.[3] Approximate integral methods, which include the HKIs and RKIs, are also based on a high-frequency approximation—the KBCs.[4]

Unlike the geometrical theories, the approximate integral methods usually give bounded results correct to within an order of magnitude, even when the boundary conditions are clearly not satisfied. Furthermore, the object can be a plane of any dimension. Figure 1 shows the source, screen, and receiver locations used in the insertion loss measurements. Figure 2 shows the errors associated with the calculation of the scattered field due to a screen of finite dimension using approximate methods. The geometric uniform theory of diffraction completely fails to predict the correct insertion loss for the low frequencies. In fact, due to its asymptotic formulation, the insertion loss is diverging to infinity as the frequency approaches zero. Clearly, applying the geometrical method to a multiple screen diffraction problem involving objects of this size would lead to a compounding of significant errors. For the cases when geometrical methods fail, a multiple screen diffraction model based on the approximate integral method would be most useful. However, the approximate integral methods are restricted to describing only single planar objects. The KBCs would have to be modified to make allowances for the description of the total field on more than one screen or aperture.

The analytic methods offer a more general solution to radiation problems as they solve the reduced wave equation over the object's surface without approximation (i.e., with an unapproximated set of boundary conditions). However, methods using this technique are not without limitations, as will be discussed briefly after the introduction of the Helmholtz integrals upon which they are based.

Let the surface of the object be denoted by δD, its interior volume by D, and its exterior region by E, as shown in Fig. 3. Equation (1)[5] defines the velocity potential ϕ in terms of known boundary conditions,

$$\iint_{\delta D}\left[\phi_t(q)\partial\frac{G(p,q)}{\partial \mathbf{n}_q}-G(p,q)\partial\frac{\phi_t(q)}{\partial \mathbf{n}_q}\right]ds_q$$

$$=\begin{cases}\phi_t(p)-\phi_0(p), & p\in E,\\ \Omega\phi_t(p)-\phi_0(p), & p\in \delta D,\\ -\phi_0(p), & p\in D,\end{cases} \tag{1a}$$

 0001-4966/95/97(1)/51/11/$6.00

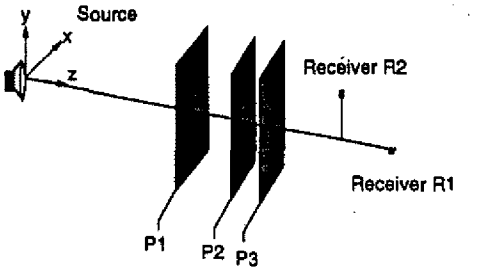

OBJECT	X (m)	Y (m)	Z (m)
Source	0.00	0.00	0.00
Receiver R1	0.00	0.00	2.65
Receiver R2	0.00	0.21	2.31
Centre of screen at P1	0.00	0.00	0.80
Centre of screen at P2	0.00	0.00	1.36
Centre of screen at P3	0.00	0.00	1.53

FIG. 1. Locations of measurement apparatus.

and,

$$\frac{\partial}{\partial \mathbf{n}_p}\int\int_{\delta D}\left[\phi_t(q)\partial\frac{G(p,q)}{\partial \mathbf{n}_q}-G(p,q)\partial\frac{\phi_t(q)}{\partial \mathbf{n}_q}\right]ds_q$$

$$=\begin{cases}\partial\dfrac{\phi_t(p)}{\partial \mathbf{n}_p}-\partial\dfrac{\phi_0(p)}{\partial \mathbf{n}_p}, & p\in E,\\ \Omega\partial\dfrac{\phi_t(p)}{\partial \mathbf{n}_p}-\partial\dfrac{\phi_0(p)}{\partial \mathbf{n}_p}, & p\in \delta D,\\ -\partial\dfrac{\phi_0(p)}{\partial \mathbf{n}_p}, & p\in D,\end{cases} \tag{1b}$$

where p is the point at which the velocity potential is to be solved, q the point of integration, and Ω the ratio of the outer solid angle solid subtended at p to 4π. The total velocity potential ϕ_t is given by the sum of a scattered component ϕ_s and an unobstructed component ϕ_0;

$$\phi_t(p)=\phi_s(p)+\phi_0(p). \tag{2a}$$

The free-space Green's function is given by

$$G(p,q)=\frac{1}{4\pi}\frac{e^{ik|p-q|}}{|p-q|}, \tag{2b}$$

where the wave number is defined as

$$k=\frac{2\pi f}{c}, \tag{2c}$$

where f and c are the frequency and velocity of the wave in free space, respectively.

Typically, Eq. (1) is used in a two-pass process to determine the field at an arbitrary point in space. First, the surface distribution is determined using Eq. (1) ($p\in\delta D$) subject to a set of boundary conditions. Once the surface distribution is known, then it is possible to compute the field for an arbitrary point in free space ($p\in E$), again using Eq. (1). Generally, there is no closed-form solution for a body of arbitrary shape. Consequently, the surface distribution is computed over enough points so that the premise for numerical integration remains valid, i.e., magnitude and phase are approximately constant over the area element. For high frequencies, where the magnitude and phase may vary significantly with small changes in distance, a very large number of integration points may have to be used, resulting in excessive computation times.

Solving Eq. (1) subject to a complete set of boundary conditions is known as the Helmholtz integral equation method (HIEM). For infinitely thin rigid planar objects, the method requires treatment of a very singular pole, third order, in the domain of integration. Terai[3] has shown that this can be treated as the sum of three terms which do not require special attention. The HIEM applied to a noninfinitely thin object (i.e., three-dimensional) suffers from nonuniqueness that occurs at frequencies that correspond to the characteristic frequencies of the internal problem. Many methods have been developed for eliminating the spurious results at the characteristic frequencies.[6–11]

There is a need for a simple method capable of describing the field at frequencies where the geometrical methods fail and where the computing time of the analytical methods applicable to two- and three-dimensional objects becomes too great. In this paper, an approximate integral method is developed to describe multiple two-dimensional object diffraction based on a set of approximate boundary conditions called the modified Kirchhoff boundary conditions. It is shown that they decouple the N by N set of simultaneous equations that define the surface potential of the analytic solution. The method suffers from neither spurious results nor the complexity of a highly singular integrand and is capable of describing thin planar objects of finite dimension. The

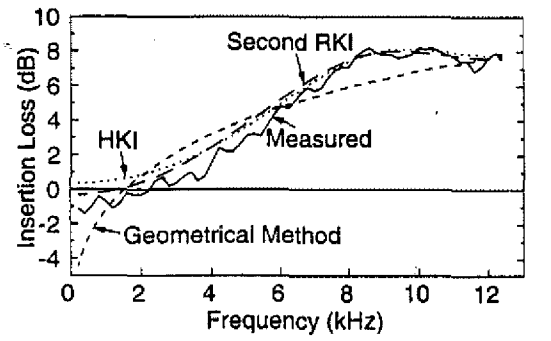

FIG. 2. Comparison of approximate methods for determining the insertion loss of a single 0.4×0.4 m screen located at $P1$ with the receiver at $R1$. The geometric calculation used the uniform theory of diffraction (Ref. 2).

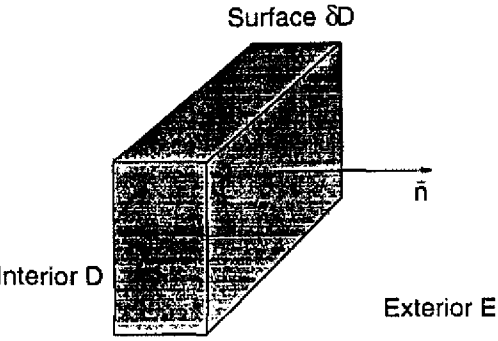

FIG. 3. Solid object and its surfaces used in the discussion.

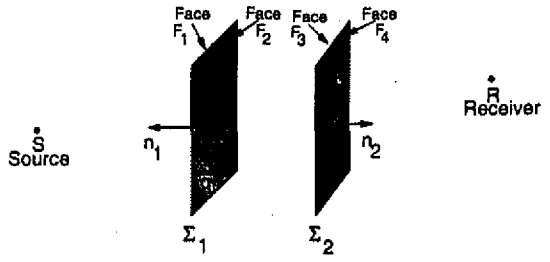

FIG. 4. Geometry for two-dimensional screens (surfaces Σ_1 and Σ_2) used in the discussion.

method is used to predict the insertion loss due to multiple two-dimensional objects or screens of finite dimension. The predicted results are compared to the measured results and are found to be in good agreement.

I. EQUATION FORMULATION

For the purpose of development, we consider two perfectly thin, flat and rigid screens as shown in Fig. 4. The acoustic wave propagates from the point source located at S to the receiver R. The velocity potential on the rigid surface is given by

$$\int\int_{\delta D} \phi_t(q)\,\frac{\partial G(p,q)}{\partial \mathbf{n}_q}\,ds_q=\frac{1}{2}\,\phi_t(p)-\phi_0(p) = \phi_s(p), \quad p\in\delta D, \tag{3a}$$

$$\int\int_{\delta D} \phi_t(q)\,\frac{\partial^2 G(p,q)}{\partial \mathbf{n}_q}\,ds_q=\frac{1}{2}\,\phi_t, \quad p\in\delta D, \tag{3b}$$

where $\delta D=\Sigma_1+\Sigma_2$. The integration is performed over both screen Σ_1 and Σ_2, but each screen has two faces with normals differing in direction by π radians. Equation (3) represents a set of coupled simultaneous equations. Equation (3b) requires special treatment before it can be applied as it has a highly singular pole of the order r^{-3} in the domain of integration. Terai[3] has shown that it can be replaced by the sum of three integrals. We focus our attention on Eq. (3a) as the introduction of approximate boundary conditions will allow us to use Eq. (3a) alone to describe the surface potential, thereby removing the problems associated with the singular integrand of Eq. (3b).

Equation (3a) is expanded in terms of the surface potentials on each face (see Fig. 4):

$$\frac{1}{2}\,\phi_t(p)-\phi_0(p)=\int\int_{\Sigma_1+\Sigma_2} \phi_t(q)\,\frac{\partial G(p,q)}{\partial \mathbf{n}_q}\,ds_q, \quad p\in dD, \tag{4a}$$

which gives

$$\tfrac{1}{2}\,[\phi_t(p_1)-\phi_t(p_2)]-\phi_0(p) = \int\int_{S_1} [\phi_t(q_1)-\phi_t(q_2)]\,\frac{\partial G(p,q)}{\partial \mathbf{n}_{q_1}}\,ds_q, \quad p\notin q\in S_1, \tag{4b}$$

$$\tfrac{1}{2}\,[\phi_t(p_3)-\phi_t(p_4)]-\phi_0(p) = \int\int_{\Sigma_2} [\phi_t(q_3)-\phi_t(q_4)]\,\frac{\partial G(p,q)}{\partial \mathbf{n}_{q_4}}\,ds_q, \quad p\notin q\in\Sigma_2, \tag{4c}$$

$$\tfrac{1}{2}\,[\phi_t(p_3)-\phi_t(p_4)]-\phi_0(p) = \int\int_{\Sigma_1} [\phi_t(q_1)-\phi_t(q_2)]\,\frac{\partial G(p,q)}{\partial \mathbf{n}_{q_1}}\,ds_q, \quad \begin{cases} p\in\Sigma_2, \\ q\in\Sigma_1, \end{cases} \tag{4d}$$

$$\tfrac{1}{2}\,[\phi_t(p_1)-\phi_t(p_2)]-\phi_0(p) = \int\int_{\Sigma_2} [\phi_t(q_3)-\phi_t(q_4)]\,\frac{\partial G(p,q)}{\partial \mathbf{n}_{q_4}}\,ds_q, \quad \begin{cases} p\in\Sigma_1, \\ q\in\Sigma_2, \end{cases} \tag{4e}$$

where p_1 is the point at which velocity potential is to be determined on face F_1, and q_1 the point of integration on face F_1 having normal n_1. Also, let the point p lie inside the object and be the point to which the field points on opposite faces converge. The subscripts follow for the other faces. To decouple Eq. (4) which defines the surface potential, consider the following discussion.

Let the disturbance have a sufficiently small wavelength that the Kirchhoff boundary conditions are valid; that is, the disturbance on the "dark side" of each screen will be zero. This allows for the immediate simplification of Eq. (4) as now the surface potentials only need to be defined on a single face of each screen. Using the fact that the normal derivative of the free-space Green's function is zero when both p and q are coplanar, we get

$$\frac{1}{2}\,\phi_t(p)-\phi_0(p)=0, \quad \begin{cases} p \text{ and } q\in\Sigma_1 \\ p \text{ and } q\in\Sigma_2, \end{cases} \tag{5a}$$

$$\frac{1}{2}\,\phi_t(p)-\phi_0(p)=\int\int_{\Sigma_1} \phi_t(q)\,\frac{\partial G(p,q)}{\partial \mathbf{n}_q}\,ds_q, \quad p\in\Sigma_2, \quad q\in\Sigma_1, \tag{5b}$$

$$\frac{1}{2}\phi_t(p)-\phi_0(p)=\int\int_{\Sigma_2}\phi_t(q)\frac{\partial G(p,q)}{\partial \mathbf{n}_q}ds_q,$$

$$p\in\Sigma_1,\quad q\in\Sigma_2. \tag{5c}$$

where we have dropped the subscripts for the integration and field points and the normals have been taken to face away from the other screen.

Equations (5) represent a set of approximate coupled simultaneous equations. To decouple the set of simultaneous equations, consider the following geometrical discussion. Let the term "disturbance" mean velocity potential (ϕ); let Σ_1 define screen 1, and let Σ_2 define screen 2. As given by Eq. 2(a), the disturbance on Σ_1 will be the sum of components from the direct wave ϕ_0 and a scattered component ϕ_s. Since Σ_1 is planar, there is no scattered component from points on Σ_1 [by Eqs. (3) and (5a)]. However, Σ_1 does experience a scattered component from Σ_2. Employing geometrical concepts, the wave propagating from the source, as shown in Fig. 4, will have been diffracted $2n+1$ times before it reaches Σ_1, where n is the multiple number ($n=1...\infty$). Again using an argument from the geometrical theories of diffraction, the field is attenuated by approximately the wave number $(k)^1$ after each diffraction by a large screen. Thus the scattered energy at the first screen which is due solely to a backscattered component from Σ_2 will be down by approximately $k^{(2n+1)}$. Thus for moderate to high frequencies, the contribution due to multiples can be considered negligible, unless a low-order multiple facilitates a direct path to the receiver. By the same procedure, it can be argued that if a scattered component on Σ_2 is to be considered, it would be due solely to the component from Σ_1 and the effects of multiple scattering should be ignored.

These arguments give the following boundary conditions and definitions of the surface potentials:

$$\tfrac{1}{2}\phi_t(p)=\phi_0(p),\quad p\in\Sigma_1, \tag{6a}$$

and

$$\tfrac{1}{2}\phi_t(p)=\phi_0(p)+\int\int_{\Sigma_1}\phi_t(q)\frac{\partial G(p,q)}{\partial \mathbf{n}_q}ds_q,\quad \begin{cases}p\in\Sigma_2,\\ q\in\Sigma_1.\end{cases} \tag{6b}$$

Equation (6a) is simply twice the KBC for a point in an aperture (aperture 1) that is defined by a rigid screen. Equation (6b) is the sum of an unobstructed component and a scattered component where the scattered component is the second RKI evaluated over the first screen. Using Babinet's principle (the unobstructed disturbance at a point p is the sum of the disturbances from the aperture and a complementary aperture that replaces the screen), Equation (6b) can be interpreted as being twice the field at a point in free space due to an aperture defined by screen 1. The factors of 2 arise from the fact that we have constrained the point of observation to lie on a screen surface. Due to the similarity to the KBC for an aperture and the RKIs, Eq. (6) will be called the modified Kirchhoff boundary conditions. An approximation of the total disturbance for an arbitrary point in space ($p\in E$) with an infinitely hard planar screen(s) present is given by applying the MKBCs to Eq. (1a).

It can be shown that the method of MKBC decouples the N by N set of equations of the HI [Eq. (1a)]. Let there be a single point of integration on each screen. There could be any number, but a single point is sufficient for illustration. Let point a be located on Σ_1, and point b on Σ_2. Equation (1a) is therefore a set of 2 by 2 simultaneous equations as shown below:

$$\begin{aligned}\phi_t(a)&=2\phi_0(a)+2\int\int_{\Sigma_1}\phi_t(a)\frac{\partial G(a,a)}{\partial \mathbf{n}_a}ds_a\\&\quad+2\int\int_{\Sigma_2}\phi_t(b)\frac{\partial G(a,b)}{\partial \mathbf{n}_b}ds_b,\\ \phi_t(b)&=2\phi_0(b)+2\int\int_{\Sigma_1}\phi_t(a)\frac{\partial G(b,a)}{\partial \mathbf{n}_a}ds_a\\&\quad+2\int\int_{\Sigma_2}\phi_t(b)\frac{\partial G(b,b)}{\partial \mathbf{n}_b}ds_b.\end{aligned} \tag{7}$$

Equation (7) is discretized as if it were being numerically integrated:

$$\begin{aligned}\phi_t(a)&=2\phi_0(a)+2\phi_t(a)\frac{\partial G(a,a)}{\partial \mathbf{n}_a}dA_a\\&\quad+2\phi_t(b)\frac{\partial G(a,b)}{\partial \mathbf{n}_b}dA_b,\\ \phi_t(b)&=2\phi_0(b)+2\phi_t(a)\frac{\partial G(b,a)}{\partial \mathbf{n}_a}dA_a\\&\quad+2\phi_t(b)\frac{\partial G(b,b)}{\partial \mathbf{n}_b}dA_b.\end{aligned} \tag{8}$$

Collecting like terms and expressing them in a matrix form we get

$$\begin{vmatrix}1-\dfrac{2\partial G(a,a)dA_a}{\partial \mathbf{n}_a} & -2\dfrac{\partial G(a,b)dA_b}{\partial \mathbf{n}_b}\\ -2\dfrac{\partial G(b,a)dA_a}{\partial \mathbf{n}_a} & 1-\dfrac{2\partial G(b,b)dA_b}{\partial \mathbf{n}_b}\end{vmatrix}\begin{vmatrix}\phi_t(a)\\ \phi_t(b)\end{vmatrix}=\begin{vmatrix}2\phi_0(a)\\ 2\phi_0(b)\end{vmatrix}. \tag{9}$$

Thus far, no assumptions have been made about the object. However, if the object is planar then the second term of element (1,1) is zero, so too is that of element (2,2). Applying the arguments used to formulate the MKBCs, the second term of element (1,2) is zero since we have assumed that Σ_2 does not contribute to the field experienced at Σ_1. Expressing the remaining terms by their definite integrals gives

$$\phi_t(a)=2\phi_0(a) \tag{10a}$$

and

$$\phi_t(b)=2\phi_0(b)+2\int\int_{\Sigma_1}\phi_t(a)\,\frac{\partial G(b,a)}{\partial \mathbf{n}_a}\,ds_b. \qquad (10b)$$

Thus the MKBCs decouple the Helmholtz integral equations by using a high-frequency approximation based on the KBC for a single planar screen or aperture. Equation (10a) is just twice the KBC. Equation (10b) is twice the second RKI and can be thought of as being twice the disturbance that would have been experienced in free space if a screen were placed between it and the source. The factors of 2 arise because it is assumed that the point p at which Eq. (10) is evaluated lies on a surface and hence there is a mirror image present. The disturbance for a point in free space is given by applying the MKBCs to the HI. The expanded equation for an arbitrary point in space (R) exterior to the objects ($R \in E$) is given by applying Eq. (6) to Eq. (1a), with the result:

$$\begin{aligned}\phi_t(R)=\phi_0(R)&+2\int\int_{\Sigma_1}\phi_0(q)\,\frac{\partial G(s,q)}{\partial \mathbf{n}_1}\,ds_q\\&+2\int\int_{\Sigma_2}\phi_0(p)\,\frac{\partial G(s,p)}{\partial \mathbf{n}_2}\,ds_p\\&+\int\int_{\Sigma_2}\left[2\int\int_{\Sigma_1}2\phi_0(q)\,\frac{\partial G(s,q)}{\partial \mathbf{n}_1}\,ds_q\right]\\&\times\frac{\partial G(p,R)}{\partial \mathbf{n}_2}\,ds_p. \qquad (11)\end{aligned}$$

As expected from Eq. (2a), the total disturbance is the sum of an unobstructed component [the first term in Eq. (11)] and one or more scattered components (the remaining terms). The second and third terms of Eq. (11) are just the RKI describing the scattered components that would be experienced at the point of observation (R) if the screen(s) were apertures. The final term may be thought of as the scattered component from the second object due to a scattered component from the first (the term contained between the brackets).

II. LIMITING CONDITIONS

Consider the result of Eq. (11) when the source and observer are on opposite sides of both Σ_1 and Σ_2 as shown in Fig. 2, under the following conditions:

(1) $\Sigma_1 \to 0$: The effect of the first screen vanishes. The second term tends to zero so too does the fourth. The resulting equation is just the RKI evaluated over Σ_2 expressing the disturbance at R due to the presence of the screen Σ_2.

(2) $\Sigma_2 \to 0$: The effect of the second screen vanishes. The third term tends to zero so too does the fourth. The resulting equation is just the RKI evaluated over Σ_1 expressing the disturbance at R due to the presence of the Σ_1.

(3) Σ_1 and $\Sigma_2 \to 0$: It follows from the above that the second, third and fourth terms will tend to zero leaving just the unobstructed component.

(4) Σ_1 and Σ_2 coplanar: Since Σ_1 and Σ_2 are coplanar, so too are the points p and q. Since the normal derivative of the Green's function is zero for coplanar points, the last term in Eq. (6b) is zero. The remaining integrals can be expressed as a single surface integral over the screen.

(5) Σ_1 and Σ_2 crossed: There exist a finite number of points along the line of intersection between Σ_1 and Σ_2. These points are contained in both Σ_1 and Σ_2 and are therefore singular points in the domain of integration of Eq. (6b). The singularity only occurs when $p=q$ and can consequently be removed by using Eq. (6a) under these conditions.

(6) $\Sigma_1 \to \infty$: The second term becomes minus the unobstructed and cancels with the first term. The expression contained in the brackets of the last term becomes minus the unobstructed at the point p on the second screen. The result is no field at the observer.

(7) $\Sigma_2 \to \infty$: Invoking the reciprocity theorem of Kirchhoff, the last term becomes minus the second, thus canceling, while the first and third terms cancel. The result is no field at the observer.

The method of MKBC is based on the high-frequency approximation of the KBC. Consequently, we expect it to perform better in the high frequencies where the boundary conditions are more likely to be satisfied. As will be shown, the approximation is quite good, even when the wavelength of the disturbance is similar to the object's dimension. For objects that are quite close together, the number of integration points will have to be chosen such that the premise for numerical integration is valid (magnitude and phase approximately constant across each integration area element). This might require a significant number of points for very small separations.

III. EQUATION SIMPLIFICATION

The disturbance at a point in free space, given by Eq. (11), involves a quadruple integral (a surface integral of a surface integral) in addition to two surface integrals. Since there is generally no closed-form solution, numerical methods must be employed, making the process very time consuming. It would be highly desirable to reduce the surface integrals to a lower order, that is, a line integral around the rim of the aperture. Maggi and later Robinowitcz have stated that the HKI can be reduced to a line integral.[12] However, when a similar procedure is applied to the Rayleigh integrals, the method fails because a perfect differential can not be formed in the new coordinate system. Terai[3] used an image point source to construct a perfect differential. This has the effect of transforming the Rayleigh integral into the HKI. It has been shown[13] that the HKI is just the mean of the first and second RKIs. Consequently, it can be shown that either of the RKIs can be replaced by the HKI without undue error when the two RKIs are approximately equal. This occurs when

$$|\overline{sq}| \approx |\overline{qR}|, \qquad (12a)$$

or

$$|\overline{sq}| \quad \text{and} \quad |\overline{qR}| \gg 1/k, \qquad (12b)$$

where $|\overline{sq}|$ is approximately equal to the source–object distance and $|qR|$ is approximately equal to the object–receiver distance for small objects. Thus when either Eqs. (12a) or 12(b) are satisfied for the appropriate boundary condition, the RKI can be replaced by the HKI and consequently the Maggi transform of the HKI. The Maggi transformation is given by

$$\phi(p)=\epsilon\phi_0(p)-\frac{1}{4\pi}\int_\Gamma \mathbf{a}\cdot\mathbf{t}\,dl, \tag{13a}$$

where

$$\mathbf{a}=\frac{e^{ik(r_0+r_1)}}{r_0r_1}\frac{\mathbf{r}_0\times\mathbf{r}_1}{r_0r_1+\mathbf{r}_0\cdot\mathbf{r}_1}, \tag{13b}$$

where

$$\mathbf{r}_0=qs, \quad \mathbf{r}_1=qp, \tag{13c}$$

and where $\mathbf{t}$ is the tangent to the rim Γ. The boolean ϵ is 1 when the line connecting the source and the point of observation intersects the radiating surface; otherwise, it is zero. By comparing the results of the HKI and RKI shown in Fig. 2, it can be seen that for the objects and orientations considered here, Eq. (12) is a good approximation. Substituting Eq. (13) into Eq. (11) gives

$$\begin{aligned}\phi(R)=\phi_0(R)(1-\epsilon_1+\epsilon_2-\epsilon_3)+\frac{1}{4\pi}\int_{\Gamma_1}\mathbf{a}_1\cdot\mathbf{t}_1\,dl\\ -\frac{1}{4\pi}\int_{\Gamma_2}\mathbf{a}_2\cdot\mathbf{t}_2\,dl+\frac{\epsilon_3}{4\pi}\int_{\Gamma_2}\mathbf{a}_2\cdot\mathbf{t}_2\,dl\\ \times\int\int_{\Sigma_2}\left(\frac{1}{4\pi}\int_{\Gamma_1}\mathbf{a}_1\cdot\mathbf{t}_1\,dl\right)\frac{\partial G(R,p)}{\partial\mathbf{n}_p}\,ds_p.\end{aligned} \tag{14}$$

For the screens and geometries considered here, the line between the source and observation points always intersects the radiating surface, so

$$\epsilon_1=\epsilon_2=\epsilon_3=1. \tag{15}$$

Substituting the values given in Eq. (15) into Eq. (14) gives the following simple description for the cases considered here:

$$\begin{aligned}\phi(R)=\frac{1}{4\pi}\int_{\Gamma_1}\mathbf{a}_1\cdot\mathbf{t}_1\,dl\\ +\frac{1}{4\pi}\int\int_{\Sigma_2}\left(\int_{\Gamma_1}\mathbf{a}_1\cdot\mathbf{t}_1\,dl\right)\frac{\partial G(R,p)}{\partial\mathbf{n}_p}\,ds_p.\end{aligned} \tag{16}$$

Having only two terms, a single and triple integral, Eq. (16) is much more compact. If the integration time varies directly with the number of integration points and there are N points on each edge for line integrals and N^2 are used for the surface integrals, then Eq. (16) is $2N$ times faster to evaluate than Eq. (11).

IV. LIMITATIONS AND APPLICATIONS

The method presented provides a simple method for determining the disturbance due to multiple screens. While we have expressed the parameters of the problem in terms of multiple screens, it can also be interpreted in a more conventional way as being a problem involving multiple apertures—the aperture being defined as the screen's extended plane. The only limit of integration explicitly expressed in terms of the screen is the last term of Eq. (14) as the others are expressed as contour integrals around the screen/aperture boundary.

The method presented is constrained by several limitations. First, the objects to be described must be constructed from finite two-dimensional planes as it was assumed that the normal derivative of the Green's function $G(p,q)$ was zero. Second, the KBCs must be satisfied. This restricts the method to describe disturbances whose wavelength is much less than the object's dimension. Despite these limitations, the method is less restrictive than the geometrical methods. Even if the approximate boundary conditions are not satisfied, the method still gives results that indicate the correct trend and in most cases the correct order of magnitude. This is quite unlike the geometrical method (UTD) of Fig. 2 which diverged rapidly when similar conditions were not met.

The application of the Maggi transformation to Eq. (11) introduces an additional constraint other than those given by Eq. (12). The transform fails if the point of observation lies on the edge of the geometrical shadow.[12] In that case, Eq. (11) should be used rather than the simplified method.

V. RESULTS

This section is broken into two parts. The first addresses the measurement system and the physical properties it must have if the measurements and theoretical predictions are to be compared. In the final part, measured and predicted insertion losses are directly compared and the results discussed.

A. Measurement system and basic requirements

The measurement system must reflect any explicit or implicit assumptions that were made during the formation of the MKBCs. These assumptions become requirements for the measurement system. They are

(1) source used must be a point source (i.e., omnidirectional),
(2) KBCs must be satisfied for the screen(s) considered (this also implies that the transmission loss through the screen must be sufficiently high), and
(3) screens used must behave as if they were infinitely thin.

Possible errors associated with these will be investigated in the sections following a description of the general measurement system.

1. General system

A convenient method for examining the accuracy of the theory is to compare the measured and predicted insertion loss due to a pair of screens. The measured insertion loss can be obtained by taking the ratio of the transfer functions (be-

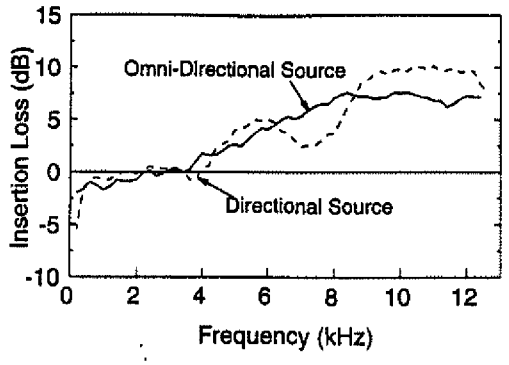

FIG. 5. The effect on single screen insertion loss due to a directional source. 0.4×0.4 m screen located at $P1$ with the receiver at $R1$.

tween the source excitation impulse and the microphone signal) with and without the screen(s) in place. The predicted insertion loss is the ratio between the predicted sound-pressure level at the receiver with and without the screen(s) in place. The measurements were conducted in an anechoic chamber to minimize the effects of room reflections. Since no anechoic room is perfectly absorptive, time gating techniques were used to remove unwanted reflections. A high-pass filter set at 200 Hz was used to remove low-frequency building noise.

2. Source

In order to compare the measured results with the theoretical predictions, which assume an ideal point source, it is necessary to construct a source that radiates energy equally in all radial directions. To illustrate this, the insertion loss for a 0.4×0.4 m screen at position $P1$ and receiver position $R1$ was measured using two different sources. The results are shown in Fig. 5. The first, a highly directional source, was a Philips AD0163 high-frequency driver having a cone diameter of about 2.5 cm mounted in a 0.14×0.14×0.25 m plywood enclosure with sharp corners. The other, a much less directional source, used the same driver but the baffle effects were reduced by locating the 0.75-cm-diameter radiating surface at the end of a long cylinder. Krishnappa[14] used a similar method.

As shown in Fig. 6, the point source was constructed from a simple hard plastic funnel cut so its mouth was just wider than the driver's radiating surface. Steel wool was placed in the mouth in an effort to offer additional damping to the driver's cone. Mineral wool was inserted in the throat to damp the standing waves that formed due to the mismatched impedance between the funnel's throat and the air outside. The driver and funnel were then encased in a thick layer of plasticine to add mass in an effort to increase the transmission loss so the energy radiated by the sides was negligible relative to that from the aperture. The shape of the encasement was smooth and slowly varying, to remove any surface discontinuities. A sharp gradient in either the surface normal or its impedance becomes a line or point source as stated by Keller's geometrical theory of diffraction. Extending the encasement to the back of the driver also improved its performance by creating a surface of homogeneous impedance. The amount of absorption in the funnel's throat was

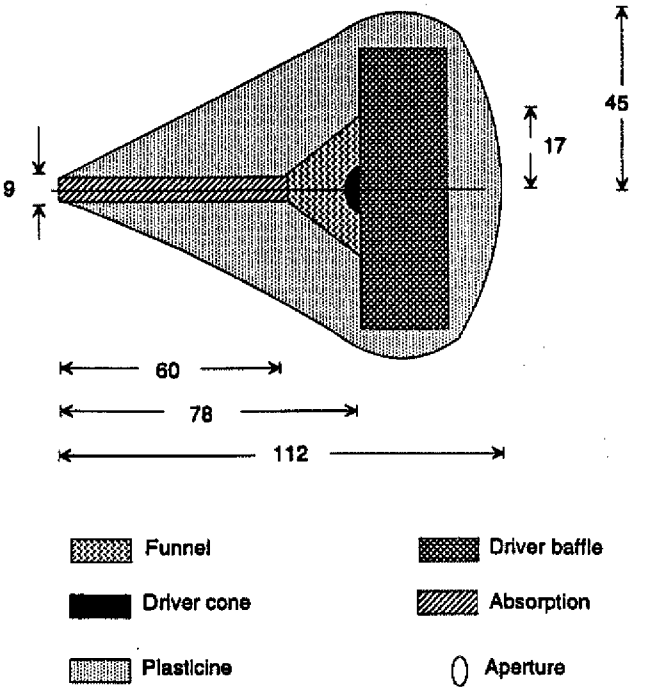

FIG. 6. Cross section of the constructed point source. Dimensions are in millimeters and are approximate.

chosen to attenuate the standing waves so that a sharp pulse could be emitted without undue smearing while maximizing the usable signal. If time gating techniques are to be used, then it is very important to have a source that has a very short-time constant so that the source does not continue to ring and emit energy after the pulse has arrived at the receiver. Several different types of driving elements were tested. The type of element that had the longest ring was a piezoelement, followed by a voice coil of a horn driver as used by Krishnappa. Of the voice coil drivers, the KEF T27 had a shorter ring than the Phillips high-frequency driver but also had lower efficiency. Since there was a small path-length difference between the chamber floor and the bottom of the screen(s), the pulse duration had to be minimized. Thus the KEF driver was chosen. Alternatively, an inverse filter could have been used to create an excitation signal that, when emitted by the driver, would produce a near-delta function.

A point source was created which radiated energy uniformly to within ±0.75 dB over a solid angle of $\pi/2$ sr for an effective frequency range of 0.2–12.8 kHz. Comparing the results shown in Fig. 5 (with the object close to the source) to those shown in Fig. 7 (with the object further away), it can be seen that the effect of source directionality is reduced as the solid angle subtended from the source by the object is diminished.

3. Objects

The two-dimensional square screens were constructed from 19-mm plywood with square edges. Three different sizes were used: 0.4×0.4, 0.5×0.5, and 0.6×0.6 m, and could be located at the three positions shown in Fig. 1. The

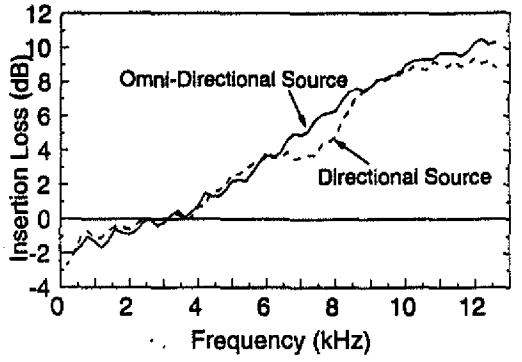

FIG. 7. The effect on single screen insertion loss due to a directional source. 0.4×0.4 m screen located at $P3$ with the receiver at $R1$.

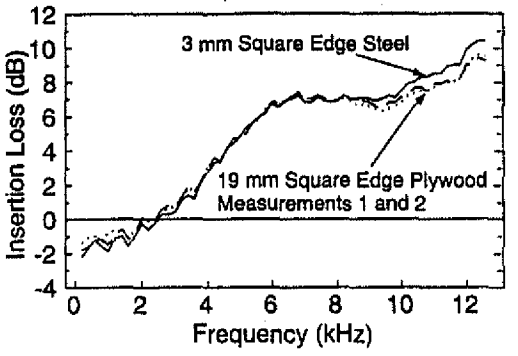

FIG. 9. Single screen insertion loss for 0.5×0.5 m screens of various thicknesses located at $P3$ with the receiver on axis at $R1$. The two measurements of the 19-mm screen were made with different time gates after the screen was removed and replaced to indicate measurement repeatability.

screens must satisfy several conditions if the predictions are to be accurately compared to the measured results.

The most basic requirement is that the screens should satisfy the KBCs upon which the MKBCs are built. This means that the disturbance on the dark side of the screen (i.e., the side not facing the source) is negligible with respect to the disturbance on the side facing the source. A further requirement is that the presence of the screen does not affect the field experienced in the extended plane of the screen (i.e., the aperture). For wavelengths that are similar to the dimensions of the screen, the disturbance on the dark side of the screen does not satisfy the KBCs as shown by Fig. 8. If the KBCs were truly satisfied, then the insertion loss for all points immediately behind the screen but displaced a very small distance would be infinite for all frequencies. The fact that the insertion loss is not infinite will be due in part to the finite transmission loss of the plywood screen especially in the low frequencies. Also, Fig. 8 shows that the KBCs are not entirely satisfied in the region defined by the extended plane of the screen (i.e., system's aperture) since the insertion loss is nonzero.

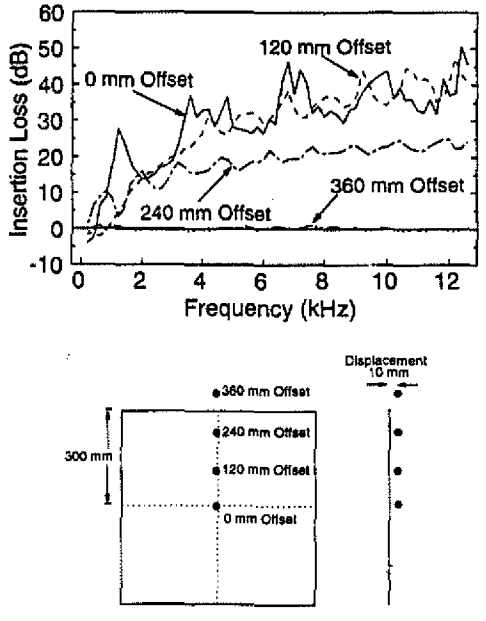

FIG. 8. Estimation of the field on the dark side of a single 0.6×0.6 m screen at $P3$. The microphone positions are located very close to the screen's surface (10 mm) to measure the sound pressure radiated by the dark side of the screen at the positions. This will provide insight to the validity of the KBCs for objects of this size.

Figure 2 which compared measured and predicted insertion losses for a single screen shows that formulation based on the KBCs overestimated the insertion loss in the low frequencies but the agreement does improve with increasing frequency. This suggests that for source, object, and receiver positions considered here, theories that use the KBCs will underestimate the sound-pressure level in the low frequencies. This may be explained by considering the KBC and MKBC assumption that there is no disturbance on the dark side of the screen(s). In reality, for wavelengths similar to the screen dimension there will most likely be a significant disturbance. Terai,[3] when he performed an analytic determination of the field on the dark side of a screen, found that even when the wavelength was about twice the object's dimension the disturbance on the dark side was comparable to that on the front. He also found that for source, object, and receiver configurations similar to those used here, the approximate KBC based method underestimated the receiver sound pressure. It is possible that when the disturbance on the dark side is summed it will tend to add in phase at the receiver, thereby reducing the insertion loss. Despite the fact the KBCs are not entirely satisfied in the low frequencies, the trend of the insertion loss curve is correctly predicted and the magnitude is usually accurate to within a few decibels for a single screen.

The other assumption of the theoretical formulation is that the screen(s) can be considered as "thin" (i.e., one whose dimension approaches zero relative to the wavelength). The insertion loss of a 19-mm plywood screen was compared to that of a 3.2-mm steel plate to determine if the plywood screens can be considered thin. The measured insertion loss for 0.5×0.5 m screen of various thicknesses is shown in Fig. 9. The results suggest that for frequencies up to about 8500 Hz the 19-mm-thick screen is behaving similarly to the much thinner 3.2-mm screen. For frequencies greater than 8500 Hz, the two screens exhibit different insertion losses with the difference apparently increasing with frequency. The plywood screen was removed and replaced and the measurement repeated with slightly different time gates to determine if the observed difference was due to measure-

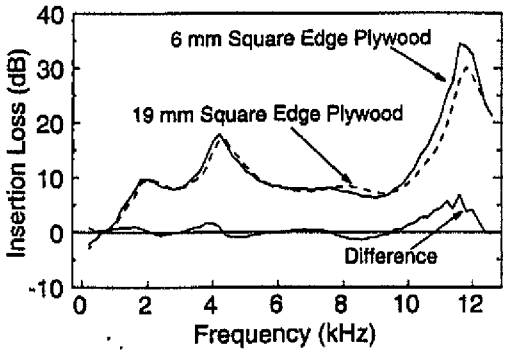

FIG. 10. Single screen insertion loss for 0.5×0.5 m screens of various thicknesses located at $P3$ with the receiver moved off-axis to $R2$. The results indicate that effect of screen thickness on measured insertion loss is a function of source, screen, and receiver location.

ment repeatability. From the figure it can be seen that the difference due to thickness is greater than the uncertainty due to measurement repeatability. Thus the observed differences are due to the finite thickness of the screens.

Figure 10 compares the measured insertion losses of a 19-mm and a 6-mm screen when the receiving point is moved off-axis. It can be seen that a significant difference between the two measured insertion losses starts near 9500 Hz and the maximum difference is nearly 7 dB. This suggests that the effect of screen thickness on the measured insertion loss is both a function of frequency and the relative positions of the object and receiver. Despite this apparent uncertainty for very high frequencies, the 19-mm plywood screen exhibits similar insertion loss trends to screens of much lesser thickness. Thus 19-mm screens prove to behave like thin screens for most frequencies of interest, and in the very high frequencies they exhibit similar insertion loss trends to screens having much less thickness.

In the formulation of the MKBCs, and consequently Eqs. (11) and (16), it was assumed that the scattered component at Σ_2 was due solely to a component which had undergone a single diffraction (i.e., multiple diffractions between Σ_1 and Σ_2 did not occur). Consequently, absorption was placed on the dark side of the screen nearest the source.

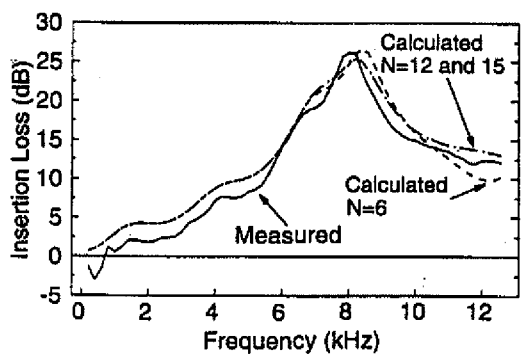

FIG. 11. Insertion loss due to two screens 0.4×0.4 m located at position $P1$; 0.4×0.4 m located at position $P2$, with the receiver at $R1$. The number of integration points on each edge, N, is varied to show the effect of under sampling.

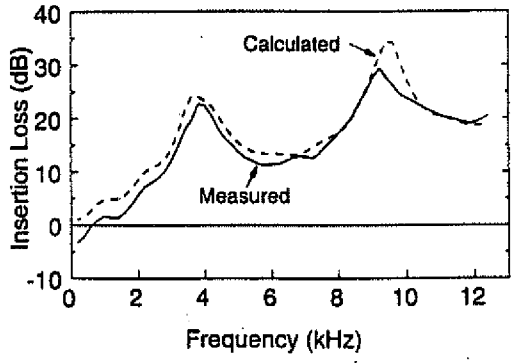

FIG. 12. Insertion loss due to two screens 0.6×0.6 m located at position $P1$; 0.6×0.6 m located at position $P2$, with the receiver at $R1$, $N=12$.

B. Comparison of measured and predicted results

Equation (16) was used to compute the insertion loss for various systems. For the purposes of numerical integration, each edge was divided into 12 segments ($N=12$), giving a total of 48 segments for line integrals and 144 for surface integrals. The location and the weighting of the integration points were determined by Gauss–Legendre quadratures. The insertion loss was computed on a 386-based 25-MHz personal computer at discrete frequencies every 200 Hz over the measurement range 200–12 800 Hz and took approximately 90 s. Screen size, location, and point of observation are changed. The predictions are compared to measured results and a method for determining the number of integration points will be given.

Figure 11 shows the measured and predicted level change due to the system of screens (0.4×0.4 m at position $P1$; 0.4×0.4 m at position $P2$; receiver position $R1$). The predicted results show the correct trends in the frequency response of the insertion loss, but the predicted results consistently overestimate the insertion loss. The overestimation can be as much as 3 dB. The predictions computed using three different numbers of integration points show that it is necessary to correctly choose the number of points as undersampling will affect the high-frequency results. Figure 12 shows that increasing both screens' size to 0.6×0.6 m does not affect the agreement. In both cases the model tends to overestimate the insertion loss in the low frequencies (i.e., when the wavelength is comparable to the object's dimension). This is due to the high-frequency approximation of the KBCs upon which the MKBCs are based. As was shown in Fig. 2 (for a single screen), the KBCs and hence the MKBCs become a better approximation to the true field potential on the dark side of a screen as the frequency increases. The fact that there are now two screens is likely to compound this error. Differences between measured and predicted results for frequencies greater than 8000 Hz may be due to the finite thickness of the screens. The thickness effects for a single screen, shown in Figs. 9 and 10, will be compounded since the system consists of two screens.

The method presented does not suffer from spurious results at the eigenfrequencies of the space between the two objects as shown by the smooth continuous curves. For the

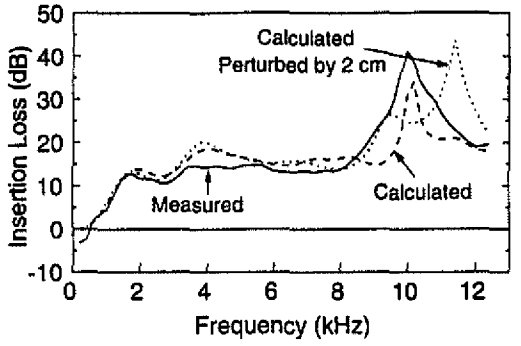

FIG. 13. Insertion loss due to two screens 0.5×0.5 m located at position $P1$; 0.5×0.5 m located at position $P3$, with the receiver at $R2$, $N=12$.

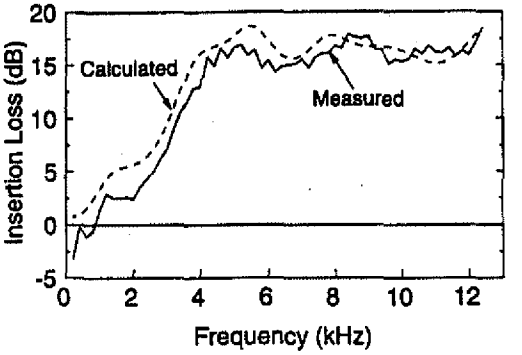

FIG. 15. Insertion loss due to two screens 0.6×0.6 m located at position $P1$; 0.4×0.4 m located at position $P2$, with the receiver at $R1$, $N=12$.

case when screens are located at positions $P1$ and $P2$, the fundamental frequency is approximately 310 Hz.

Figure 13 shows that the measured and predicted insertion losses for an off-axis point of observation (i.e., receiver position $R2$). For frequencies up to 9 kHz, the measured and predicted results agree within about 4 dB (with the prediction showing a higher insertion loss). After 9 kHz, the prediction only follows the general trend of the measured insertion loss. The difference between measured and computed may be due to the screens' finite thickness and also the uncertainty in the true relative positions of the source, screens, and receiver. Uncertainties in the object's position can significantly alter both the phase and magnitude of the predicted disturbance on the objects and ultimately the sound-pressure level at the receiver. To illustrate the sensitivity of the insertion loss on the screens' position, the computer model was run with the screens' position shifted by 2 cm in the positive Y direction. Figure 13 shows a significant insertion loss change for frequencies greater than 9000 Hz. This effect should not be unexpected since shifting the screens by 2 cm represents a change in position by more than $\lambda/2$ at 9000 Hz. Ideally, detailed measurements made as a function of small perturbations would be used to evaluate this effect. However, such data are not available at the present time.

Thus far, only two screens of uniform size have been used. Now the case when the screens are of unequal size is considered. Figure 14 shows the result when there is a 0.4 ×0.4 m screen at position $P1$ and a 0.6×0.6 m screen at position $P3$. Agreement is very good, less than 2 dB difference, for the range 6–12.8 kHz, while for frequencies less than 6 kHz, the trend and details of the insertion loss are correctly represented by the prediction which is within 3 dB of the measured. In Fig. 15, the screens are interchanged and the degree of agreement remains similar. That is, the prediction tends to overestimate the insertion loss. The difference is typically less than 3 dB for frequencies below 6 kHz. For frequencies above 6 kHz both the trend and magnitude are correctly predicted. It is interesting to note that the level change during the first 4 kHz is very similar.

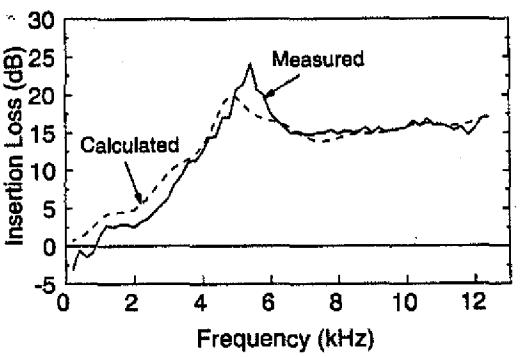

FIG. 14. Insertion loss due to two screens 0.4×0.4 m located at position $P1$; 0.6×0.6 m located at position $P2$, with the receiver at $R1$, $N=12$.

C. Determining the number of integration points

Selecting an adequate number of numerical integration points is critical to attaining a prediction that is not contaminated in the high frequencies. Figure 11 has already shown the significant effect that using insufficient integration points can have on results. The number of points required will be a function of the frequency, the size of the screens, and the geometry between the source (either the point source or a field point on a screen) and the receptor points. Figure 16 shows two adjacent receptor points p_1 and p_2 having distances r_1 and r_2 to the field point s. In general, the following must hold:

$$r_2 - r_1 \ll \delta, \tag{17}$$

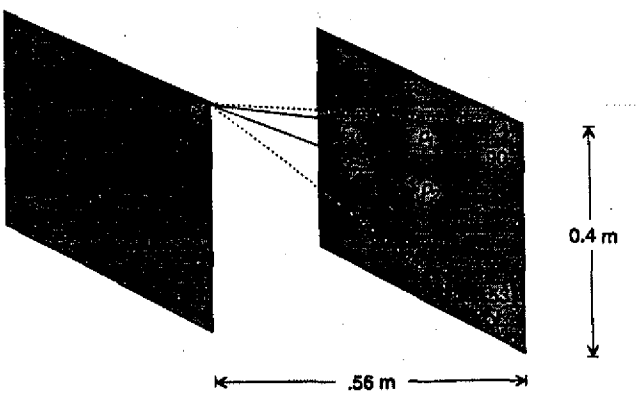

FIG. 16. Sketch showing integration points and the screen geometries used in determining the number of integration points for the 0.4×0.4 m screens located at positions $P1$ and $P2$ of Fig. 11.

where δ is some fraction of a wavelength. If the Nyquist sampling theorem is applied, then $\delta=\lambda/2$. If the angle between the line r_1 and plane is θ, then Eq. (17) can be rewritten as

$$(r_1^2+d^2\sin^2\theta)^{1/2}+d\cos\theta-r_1=\delta=\lambda/2. \quad (18)$$

Ideally, this would hold for all angles of θ that are applicable to the system. For the geometry of the two screen system of Fig. 11, the range of angles is quite limited. The largest range occurring with the source on the first screen and the receptor points on the second screen is shown in Fig. 16. In this case, the range is approximately 53°–90°. Figure 11 showed that with 6 points used for the line integrals and 36 for the surface integrals, the error due to under sampling begins at about 6200 Hz. Using the wavelength at 6200 Hz (0.0553 m), Eq. (18) suggests that there should be less than nine points on each edge ($\theta=53°$) but more than three points ($\theta=90°$). Using nine points on each edge would satisfy the condition [Eq. (18)] for the range of angles $53°\leqslant\theta\leqslant90°$ but appears to be too conservative when the observed results of Fig. 11 indicated that only six points were required. However, the mean of the two extremes (three points and nine points) represents a number which is in good agreement with the observed requirement of six points on each edge. This method requires further work to determine its applicability to more general geometries.

VI. CONCLUSIONS

The method of MKBC based on the KBCs has proved to be effective in predicting the surface potential on multiple two-dimensional objects. The MKBCs, when applied to the HIEM, decouple the N by N set of simultaneous equations. The resulting expressions for the surface potential can easily be integrated as there are no poles in the domain.

Experimentally the method was shown to offer a reasonable prediction of the disturbance at a point in space when there were two intervening screens. However, the method did suffer from the limitations associated with the KBCs upon which it is based. This was characterized by the method underestimating the sound-pressure level at the receiver in the low frequencies (hence an overestimation of the screens' insertion loss). Despite this, the correct insertion loss trends were exhibited and the agreement tended to improve with frequency. Experimental work revealed that the 19-mm square edge screens used could not be considered "infinitely thin" for frequencies greater than about 8500 Hz as the thickness began to affect insertion loss. The effect of screen thickness was most pronounced for receiver positions off-axis. The screens' finite thickness may have contributed to the deviation between measured and predicted results in the high frequencies. The insertion loss was shown to be greatly effected by shifts in position when distance $\lambda/2$ or greater.

The MKBCs provide a convenient alternative, especially for objects and frequencies that are not well suited to either the geometrical theories of diffraction or the analytic methods. The method of MKBC forms the basis for describing a special class of diffraction problems.

ACKNOWLEDGMENTS

The efforts of Professor Robert Craik, Heriot Watt University, Scotland and the members of the Institute for Research in Construction, National Research Council Canada, especially those of Dr. John Bradley, are acknowledged.

[1] J. Keller, "Geometrical theory of diffraction" J. Opt. Soc. Am. **52**(2), 116–130 (1962).
[2] R. G. Kouyoumjian, and P. H. Pathak, "A uniform geometrical theory of diffraction for an edge in a perfectly conducting surface," Proc. IEEE **62**, 1458–1461 (1974).
[3] T. Terai, 1980, "On the calculation of sound fields around three dimensional objects using integral equation methods," J. Sound. Vib. **69**(1), 71–100 (1980).
[4] C. J. Bouwkamp, "Diffraction theory," Rep. Prog. Phys. **17**, 35–72 (1954).
[5] A. Burton, "The solution of Helmholtz' equation in exterior domains using integral methods," National Physical Laboratory, NPL Rep. NAC 30 (1973).
[6] H. Schenck, "Improved integral formulation for acoustic radiation problems," J. Acoust. Soc. Am. **44**(1), 41–58 (1968).
[7] A. Seybert and T. Rengarajan, "The use of CHIEF to obtain solutions for acoustic radiation using boundary integral equations," J. Acoust. Soc. Am. **81**(5), 1299–1306 (1987).
[8] A. Burton and G. Miller, "The application of internal equation methods to the numerical solution of some exterior boundary value problems," Proc. R. Soc. London Ser A **323**, 201–210 (1971).
[9] W. L. Meyer, W. A. Bell, and B. T. Zinn, "Boundary integral solutions of three dimensional acoustic radiation problems," J. Sound Vib. **59**(2), 245–262 (1978).
[10] Z. Reut, "On the boundary integral methods for the exterior acoustic problem," J. Sound Vib. **103**, 297–298 (1985).
[11] K. Cunefare and G. Koopman, "A boundary element method for acoustic radiation valid for all wave numbers," J. Acoust. Soc. Am. **85**(1), 39–48 (1989).
[12] B. Baker and B. Copson, *Huygens' Principle* (Clarendon, Oxford, 1950), pp. 74.
[13] E. Wolf and E. Marchand, "Comparison of the Kirchhoff and the Rayleigh–Sommerfeld theories of diffraction at an aperture," J. Opt. Soc. Am. **54**(5), 587–594 (1964).
[14] A. Krishnappa, "Sound intensity in the near field of a point source over a hard reflecting plane," J. Acoust. Soc. Am. **82**(2), 667–678 (1987).